Thalamocortical Dynamics during Rapid Eye Movement Sleep in the Mouse Somatosensory Pathway

Flore Boscher, Katlyn Jumel, Tereza Dvorkov, Luc J Gentet, Nadia Urbain

▶ **To cite this version:**

Flore Boscher, Katlyn Jumel, Tereza Dvorkov, Luc J Gentet, Nadia Urbain. Thalamocortical Dynamics during Rapid Eye Movement Sleep in the Mouse Somatosensory Pathway. Journal of Neuroscience, 2024, 44 (25), pp.e0158242024. 10.1523/jneurosci.0158-24.2024 . hal-04760549

HAL Id: hal-04760549
https://hal.science/hal-04760549v1

Submitted on 30 Oct 2024

HAL is a multi-disciplinary open access archive for the deposit and dissemination of scientific research documents, whether they are published or not. The documents may come from teaching and research institutions in France or abroad, or from public or private research centers.

L'archive ouverte pluridisciplinaire **HAL**, est destinée au dépôt et à la diffusion de documents scientifiques de niveau recherche, publiés ou non, émanant des établissements d'enseignement et de recherche français ou étrangers, des laboratoires publics ou privés.

Systems/Circuits

Thalamocortical Dynamics during Rapid Eye Movement Sleep in the Mouse Somatosensory Pathway

Flore Boscher,[1] Katlyn Jumel,[1] Tereza Dvořáková,[1] Luc J. Gentet,[2] and Nadia Urbain[1]

[1]Physiopathology of Sleep Networks, Université Claude Bernard-Lyon 1, Lyon 69500, France and [2]Forgetting Processes and Cortical Dynamics, Lyon Neuroscience Research Center, INSERM U1028-CNRS UMR5292, Université Claude Bernard-Lyon 1, Lyon 69500, France

Rapid eye movement (REM) sleep, also referred to as paradoxical sleep for the striking resemblance of its electroencephalogram (EEG) to the one observed in wakefulness, is characterized by the occurrence of transient events such as limb twitches or facial and rapid eye movements. Here, we investigated the local activity of the primary somatosensory or barrel cortex (S1) in naturally sleeping head-fixed male mice during REM. Through local field potential recordings, we uncovered local appearances of spindle waves in the barrel cortex during REM concomitant with strong delta power, challenging the view of a wakefulness-like activity in REM. We further performed extra- and intracellular recordings of thalamic cells in head-fixed mice. Our data show high-frequency thalamic bursts of spikes and subthreshold spindle oscillations in approximately half of the neurons of the ventral posterior medial nucleus which further confirmed the thalamic origin of local cortical spindles in S1 in REM. Cortical spindle oscillations were suppressed, while thalamus spike firing increased, associated with rapid mouse whisker movements and S1 cortical activity transitioned to an activated state. During REM, the sensory thalamus and barrel cortex therefore alternate between high (wake-like) and low (non-REM sleep-like) activation states, potentially providing a neuronal substrate for mnemonic processes occurring during this paradoxical sleep stage.

Key words: **barrel cortex; electrophysiology; local field potential; REM sleep; single-unit recordings; somatosensory; spindle; thalamus; whisking**

Significance Statement

Mammalian sleep includes slow wave sleep, or non-rapid eye movement sleep (NREM), and the subsequent REM sleep (REM). At the EEG global level, cortical activity during REM sleep has long been believed to share some similarities with awake cortical activity. The well-defined mouse whisker system offers the unique opportunity to precisely investigate cortical and thalamic dynamics during wakefulness and REM. Combining local field potential recordings in primary somatosensory cortex, with single-unit neuronal recordings in its associated thalamic nucleus, we found that during REM, the sensory thalamus and barrel cortex alternate between high (wake-like) and low (non-REM sleep-like) activation states, potentially providing a neuronal substrate for mnemonic processes occurring during this paradoxical sleep stage.

Introduction

Mammalian sleep includes two main states: slow wave sleep, or non-rapid eye movement sleep (NREM), and the subsequent rapid eye movement sleep (REM). REM has long been defined as a state of fast, desynchronized, and low-voltage electroencephalogram (EEG) resembling wakefulness, with the occurrence of transient bursts of ocular movements coupled with a complete muscle atonia (Aserinsky and Kleitman, 1953; Dement, 1958). This striking EEG activation during a sleep state inspired Jouvet to coin REM with the name "paradoxical sleep" (Jouvet et al., 1959). Many further transient events co-occurring with REMs, including muscle twitches, breathing fluctuations, heart rate surges, or facial movements, associated with electrophysiological markers such as pontine P-waves or an increase in EEG and hippocampal theta frequency, have since been described (Sano et al., 1973; Sei and Morita, 1996; Karashima et al., 2005; Sato et al., 2010; Bueno-Junior et al., 2023). These phasic events appear on the background of an apparently more quiescent, tonic

Received Jan. 23, 2024; revised May 2, 2024; accepted May 13, 2024.

Author contributions: N.U. designed research; F.B. and N.U. performed research; F.B., K.J., T.D., L.J.G., and N.U. analyzed data; N.U. wrote the paper.

We thank Anne-Laure Morel, Sébastien Arthaud, and the animal facility of the CRNL for technical support. We deeply thank Imola Mihalecz and C. Balazuc for technical assistance and help with the experiments. We warmly thank M. Bodier, N. Fourcaud-Trocmé, C. Loisel, A. Legay, O. Braud, and A. Le Houssel for help with data processing and analysis. We are grateful to P. Salin and A. Hay for advices and critical reading of the manuscript. This work was funded by a Ministerial Doctoral grant (F.B.), ANR PARADOX (ANR-17-CE16-0024; N.U. and L.J.G.), and ANR Pom-Pom (ANR-21-CE16-0017; N.U.).

The authors declare no competing financial interests.

Correspondence should be addressed to Nadia Urbain at nadia.urbain@inserm.fr.

https://doi.org/10.1523/JNEUROSCI.0158-24.2024

Copyright © 2024 the authors

state, suggesting that REM is not a homogeneous sleep state (Brankačk et al., 2012; Simor et al., 2020). Indeed, local field potential (LFP) recordings of brain areas revealed the unexpected presence of local delta oscillations during REM both in humans and rodents (Tinguely et al., 2006; Funk et al., 2016; Baird et al., 2018; Bernardi et al., 2019). Delta activity had mostly been described in NREM sleep and more recently in wakefulness (Petersen et al., 2003; Vyazovskiy et al., 2011; Urbain et al., 2015; Fernandez et al., 2017). In NREM, cortical delta waves and spindles, along with sharp-wave ripples in the hippocampus, have been shown to be involved in mnemonic processes (Sirota et al., 2003; Maingret et al., 2016). Since memory consolidation and emotional processing have also been functionally ascribed to REM sleep (for review, Rasch and Born, 2013; Poe, 2017; Sara, 2017), it raises the question whether delta oscillations play a similar mnemonic function in REM. The activation of a thalamocortical network including limbic and parahippocampal areas was reported during REMs in humans (Maquet et al., 1996; Wehrle et al., 2007; Corsi-Cabrera et al., 2016; Lambert et al., 2022; Peter-Derex et al., 2023), but still very little is known about the neuronal mechanisms subtending these observations. Considering that, except in early stages of the development, spindle-like waves in REM were rarely reported in the literature (Tiriac and Blumberg, 2016; Meyer et al., 2018), it was proposed that hippocampal theta rhythm in REM may assume this role in mnemonic processes (Montgomery et al., 2008; Boyce et al., 2016).

The present study aimed at exploring cortical oscillations and their thalamic correlates associated with REM substates. Focusing on the mouse somatosensory system, we report during REM a highly dynamic interplay between local oscillations in the primary somatosensory (S1) cortex and membrane potential dynamics and neuronal firing activity of the thalamic ventral posterior medial nucleus (VPM). We (1) describe that S1-LFP displays features of NREM sleep during tonic REM, characterized by strong delta (2–6 Hz) power associated with spindles (10–18 Hz), which are suppressed during phasic periods of whisker movements, when S1-LFP transitioned to an activated state, and (2) demonstrate its thalamic neuronal correlates which confirm the thalamic origin of the observed REM spindles.

Materials and Methods

Experimental model and subject details

All procedures were approved by the "Ministère de la Recherche et de l'Enseignement Supérieur" (authorization APAFIS #35416) and were conducted in accordance with the European directive 86/609/EEC on the protection of animals used for experimental and scientific purposes. All efforts were made to minimize the number of animals used, as well as their stress and suffering. Experiments were carried out in male 8- to 16-week-old C57BL6J mice. After surgery, mice were housed individually to avoid deterioration of the implanted connector; they were weighted and handled daily. All animals were housed in standard conditions (23 ± 1°C, food and water *ad libitum*) with toys to enrich their environment. All experiments were performed during the light part of the cycle (12 h light/dark).

Method details

Surgery for head fixation. Mice were anesthetized with a solution of ketamine (100 mg/kg) and xylazine (8 mg/kg) and were positioned in a stereotaxic frame. Body temperature was monitored and maintained at 37°C with an electric heating pad and eyes were covered with Liposic to prevent from ocular dryness. The skull was exposed, carefully cleaned with Betadine, and placed horizontally. Two stainless-steel screws were implanted over parietal (−1.7 mm posterior to bregma; +1.2 to 1.9 mm lateral to midline) and frontal (+1.5 mm anterior to bregma; −1.5 mm lateral to midline) cortical areas of the right hemisphere to measure the electroencephalogram (EEG, Fig. 1*A*). Two flexible steel wires were inserted into neck muscles to monitor the electromyogram (EMG). A lightweight metal head-holder, fixed to a micromanipulator fastened to the stereotaxic frame, was glued to the skull, as well as recording chambers above the regions of interest (S1 and thalamus, M1 or hippocampus for a subset of mice) of the left hemisphere. The bone was then covered with a thin layer of acrylic cement (C&B Metabond). The metal piece was embedded in dental cement with the EEG screws, the EMG wires, and their four-pin connector. To prevent infection, a thin layer of cyanoacrylate glue was applied on the exposed skull before sealing the recording chamber with silicon cement (Kwik-Cast, World Precision Instruments). An iodine solution (Betadine 10%) was applied to all the borders of the implant for subsequent healing. Twenty minutes before the end of the surgery, the mouse received a subcutaneous injection of carprofen (5 mg/kg). Animals were allowed to recover for 5 d before habituation sessions began. The implant (∼1 g total weight, i.e., metal implant + connector + cement embedding) was well-tolerated by mice which were able to move, sleep, feed, and drink normally in their home cage.

Mice training and habituation. During 3–5 weeks, repetitive daily training sessions of increasing durations were performed to habituate the mice to the head restraint. Their head was painlessly secured by screwing the metal piece, cemented to the mouse's head to a head-fixation pillar, their body lying comfortably in a cardboard roll carpeted with soft tissue. Experimental recording sessions were initiated only when periods of quiet wakefulness, NREM, and REM were observed by the experimenter during the training sessions on the EEG/EMG recordings.

After the training period and before the first recording session, a small craniotomy was performed, under isoflurane and buprenorphine (0.05 mg/kg), over the barrel cortex (S1; anteroposterior: −1.7 mm relative to bregma, lateral: +3.5 mm relative to midline; Paxinos and Franklin, 2001) in order to target LFP recordings from layer 5. Another craniotomy (∼1 mm) was drilled over the thalamus (anteroposterior: −1.7 mm relative to bregma, lateral: +1.7 mm relative to midline). For a subset of mice, a third craniotomy was performed over the primary motor cortex (M1; anteroposterior: +1 mm relative to bregma, lateral: −1 mm relative to midline) or the hippocampus (HPC; anteroposterior: −2 mm relative to bregma, lateral: +1.2 mm relative to midline). The dura mater was then removed in all craniotomies, and the recording chambers were closed with Kwik-Cast. All whiskers except for C2 were trimmed 10–15 mm from the skin. After 3–4 h of recovery, the mouse was placed in the restraining frame as during the training sessions, and recordings were performed. Recording sessions of 3–4 h were performed every day, for 2–6 d per mouse. In order to prevent eventual food or water deprivation during head restraint, animals were fed regularly outside recording periods.

Single-unit and polygraphic recordings. LFP recordings (Grass QP511; bandpass filtered 0.1–300 Hz) were performed with glass micropipettes (6–8 µm tip diameter) filled with sodium chloride (0.15 M) and lowered into layer 5 (−600 µm) of S1 barrel at 30° angle from the vertical. Surface contact was detected under the binocular microscope and manipulator depth set at 0 µm, and the pipette was then lowered until reaching −600 µm (layer 5; Lefort et al., 2009). In some experiments, glass micropipettes were vertically lowered in layer 6 (−1,000 µm) of M1 and the CA1 region (−1,200 µm) of the HPC.

Single units in the thalamus were recorded using glass micropipettes (≤1 µm tip diameter, 30–80 MΩ) lowered vertically and filled with a solution of potassium acetate (0.5 M) and Neurobiotin (2%, Vector Laboratories). The signal was amplified and low-pass filtered (10 kHz, Cygnus, NeuroData), fed to an oscilloscope and an audio monitor, and digitized at 20 kHz. LFP and thalamic recordings were collected together with amplified EEG (bandpass filtered 0.1–300 Hz) and EMG (bandpass filtered 30–300 Hz) polygraphic signals (Grass QP511). The reference electrode for recordings with glass micropipettes was located on the surface of the skull, inside the recording chamber filled with sterile saline

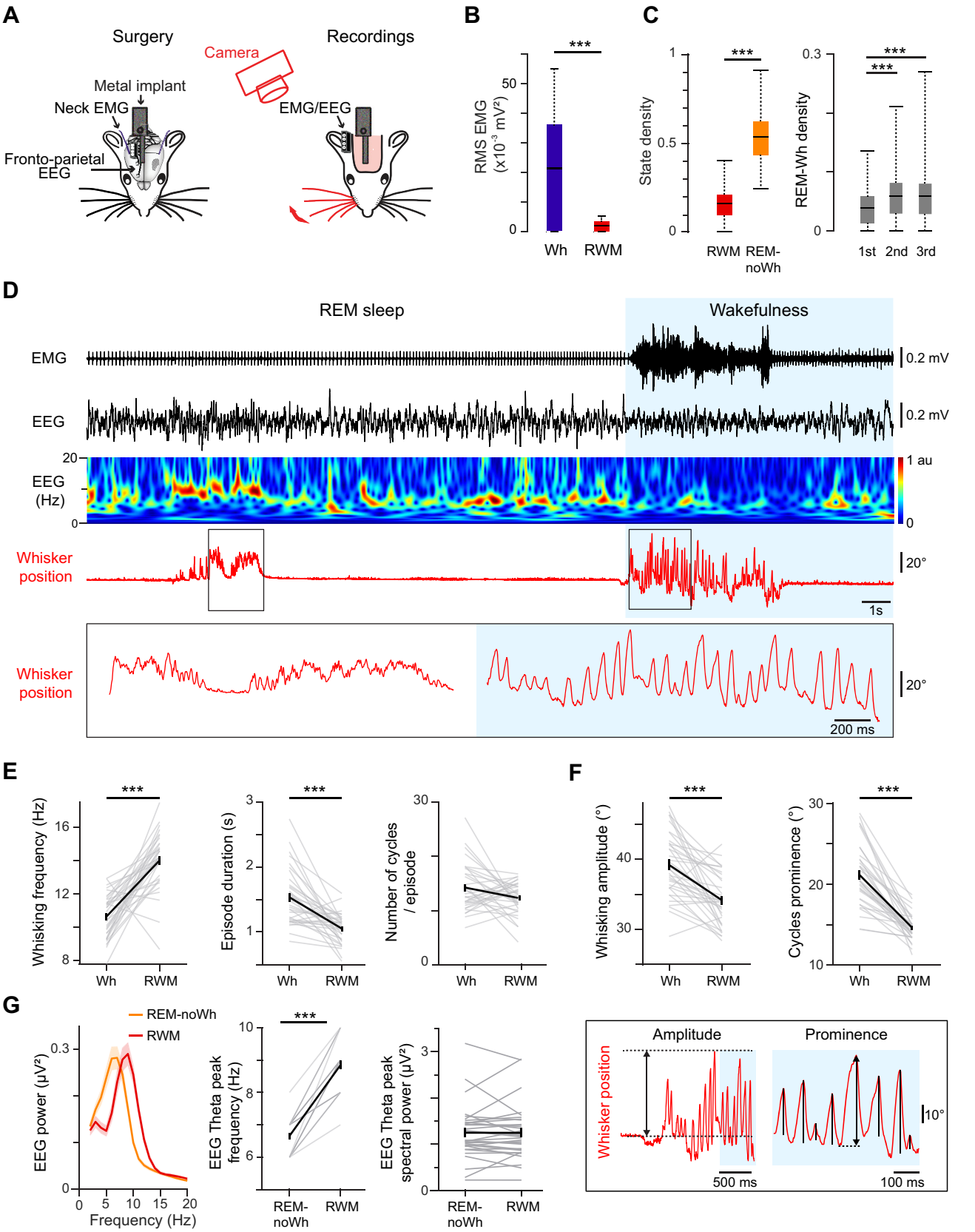

Figure 1. Phasic activity in REM sleep. ***A***, Schematic of the experimental set-up. Left, EEG and EMG electrodes were implanted and a metal head-holder was stereotaxically glued to the skull. Right, Whisker movements were filmed with a high-speed camera in parallel of EEG and EMG monitoring. ***B***, Root mean square (RMS) of the EMG from the neck muscles recorded during Wh and RWM. Boxplots indicate mean (black line) and interquartile range ($n = 42$ mice). ***C***, Left, Percentage of time spent in RWM and REM-noWh during REM episodes (see Materials and Methods for calculations). Right, Percentage of time spent in RWM during the first, second and third part of REM episodes longer than 60 s (ANOVA for repeated measures). Boxplots indicate mean (black line) and interquartile range. ***D***, Example of a typical EEG recording during REM and the subsequent awakening. Top to bottom, Neck EMG, EEG, corresponding EEG wavelet time-frequency spectrum,

solution. All signals were collected via a CED power 1401 analog-to-digital converter (Cambridge Electronic Design) using Spike2 software.

Initial localization of thalamic cells was based on the coordinates described in Paxinos and Franklin (2001). Manual deflection of individual contralateral (right side) whiskers was performed in order to determine the receptive field of recorded cells. All cells assigned to the VPM and tested for whisker deflections were mono- or multiwhisker responsive cells. Cell locations were determined by the juxta- or intracellular labeling of the last recorded cell (Pinault, 1996) and the reconstruction of each pipette track.

At the end of experiments, mice were perfused under deep anesthesia with saline, followed by a fixative containing 4% paraformaldehyde in phosphate buffer (PB 0.1 M, pH 7.3). Brains were postfixed for 1 h, and coronal slices were subsequently cut at 50 µm thickness with a vibratome. Sections were processed for cytochrome oxidase and Neurobiotin histochemistry according to standard protocols (Veinante et al., 2000).

Quantification and statistical analysis

Code accessibility. All the data as well as codes and algorithms that support the findings of this study are fully available from the corresponding author upon request.

Cortical and behavioral states. The activity of thalamic cells was recorded together with EEG and LFP in the ipsilateral S1 in layer 5 (600 mm depth). In addition, the muscle tone was monitored from the neck (EMG), and whisker movements were tracked with a high-speed camera. All these parameters allowed us to determine the vigilance state of the mouse. In this paper, we focus on cortical and thalamic activity during REM and its relationship with other vigilance states of sleep and wakefulness, specifically non-REM sleep (NREM), Whisking (Wh), and active and quiet wakefulness (respectively, aWK and qWK; Urbain et al., 2015, 2019). REM was characterized by the absence of EMG tone and a prominent peak in the theta range (6–9 Hz) in the EEG. Only the presence of whisker movements, or not, distinguished RWM from REM-noWh. In REM, whisking episodes were considered when whisker movements were at least 15° in amplitude and lasted at least 300 ms. Periods of REM with either jaw chattering, low amplitude (inferior to 15°), or short duration whisker movements (<300 ms) were not scored neither as RWM nor REM-noWh (approximately one-third of REM). NREM was distinguished by high-amplitude, low-frequency EEG and LFP (0.1–1.5 Hz) activity with a strong dominant frequency range of 10–18 Hz (spindle activity), associated with a weak EMG tone. NREM is clearly distinguishable from REM, since REM is characterized by cortical EEG spectra with a strong dominant theta band (6–9 Hz) and no muscle tone at EMG. Quiet wakefulness was defined by high-amplitude, low-frequency (2–6 Hz) EEG and LFP activity associated with a weak EMG tone; qWK is clearly distinguishable from NREM, since both cortical LFP and EEG spectra displayed in NREM strong dominant frequencies in the slow wave and spindles ranges (Urbain et al., 2015, 2019). Active wakefulness and Whisking were characterized by lower-amplitude and higher-frequency EEG and LFP oscillations than quiet wakefulness, associated with sustained EMG activity; polygraphic features of the Active and Whisking states are similar, but in the latter case the mouse was whisking. Whisking episodes in wakefulness were considered when whisker movements were at least 20° in amplitude and lasted at least 300 ms; periods of time associated with whisker movements of smaller amplitude or shorter duration were excluded from the analysis. Transitional and intermediate states (such as drowsiness or transition from NREM to REM sleep) were excluded from the analysis. Spike time occurrences were determined as threshold amplitude crossings. The spike detection was checked (and corrected if necessary) for each episode included in the analyses. An automatic scoring of these states was performed using a custom-written software in Matlab, and the detection was systematically checked manually.

Quantification of whisker movements. Electrophysiological recordings were performed while the whisker movements of the mouse were simultaneously filmed using a high-speed camera (Photonfocus MV1-D2048X1088I-96-G2) operating at 400 frames per second. Continuous recordings were performed in 600 s bouts. Whisker movements were quantified off-line using DeepLabCut interface and custom-written routines running with Python to track whisker position, measured as the angle between the nose, the attachment of the whisker to the whiskerpad, and a point on the whisker. Whisking occurrences were found using a custom-written routine running with Matlab and checked manually. Whisking amplitude of each episode was defined as the difference between the maximum whisker position and the mean angle 200 ms before. To optimize the detection of whisking cycles, whisker position was high-pass filtered at 2 Hz. Whisking cycles were then detected using the function "*findpeaks*" of Matlab, which also returned the prominence of each peak. Note that a minimum peak prominence "MinPeakProminence" was set at 5° to optimize the detection in both wakefulness and REM. However, due to the whisking kinematic in REM, described in the Results and illustrated in Figure 1, we were not able to detect all whisking cycles in REM. The number of cycles/whisking episode is therefore underestimated and the mean cycle prominence overestimated in REM compared with those measured in wakefulness.

Spectral analysis. Raw data were imported from spike2 to Matlab and processed using custom-written functions. EEG and cortical LFPs were filtered (1–256 Hz) and downsampled to 512 Hz. Signals were classified per vigilance state and 1 s epochs were selected in each state. All epochs were then collected for each mouse and each state. A Hanning window was applied to each epoch and all the analysis described in this section were computed on these 1 s epochs, precluding us from studying oscillations below 2 Hz, but allowing us to analyze short phasic events such as whisking and RWM. All epochs were averaged to get the result per mouse and per state. Power spectral density (PSD) was computed using the *mtspectrumc* function of the chronux toolbox, and the spectral power in the different frequency ranges was calculated as the sum of the PSD in the range of interest. Normalized PSD were computed by dividing the PSD by its sum between 1 and 45 Hz. Theta peak frequency was computed, for each mouse, as the frequency of the maximum value of the PSD between 5 and 12 Hz. From this value *fmax*, theta peak spectral power was computed in the range [*fmax* − 2 Hz: *fmax* + 2 Hz]. The correlation between the EEG and the HPC-LFP was computed using the functions *xcorr* in Matlab. In addition, we computed the correlation between the HPC-LFP and the randomly permuted EEG using the function *circshift (surrogates)*. This step was repeated 100 times. To assess the statistical significance of the average correlation coefficient for each mouse, we compared the amplitude of the real correlation coefficients with those of the surrogates.

In order to analyze theta/gamma modulation, theta and gamma oscillations were extracted from each signal using the Ensemble Empirical Mode Decomposition (EEMD). This method decomposes the signal into the so-called intrinsic mode functions (IMFs) that correspond to a time series of a frequency present in the signal. Selecting the IMFs with a maximum frequency in the theta (5–12 Hz) and gamma (60–90 Hz) ranges allowed us extract theta and gamma oscillations without any modifications of the raw data (no filter). Theta gamma comodulograms were examined by computing the coherence between the signal (EEG or

←

and whisker position (in red) with the enlarged view of the black boxes. Whisker movements are indeed not restricted to wakefulness. ***E***, From left to right, Whisking frequency, duration, and number of protraction/retraction cycles per episode, in wakefulness, and REM. ***F***, Average whisking amplitude (left) and prominence (right) per mouse, in wakefulness and REM, with an illustration of the method used to estimate these parameters (bottom). ***G***, Grand average PSD of the EEG during REM sleep with (red) or without (orange) whisker movements (left) and corresponding averaged EEG theta peak frequency (middle) and spectral power (right) per mouse. ***C***, ***G***, $n = 32$ mice; data were compared using Wilcoxon or Friedman tests (***G***, see Extended Data Table 1-1 for additional statistical measures). ***E***, ***F***, $n = 35$ mice; *t* test for paired data. Mean ± SEM in black. Note that *y*-axes do not start at "0."

HPC-LFP) and gamma power time series for each frequency (bin 1 Hz; Sirota et al., 2008). Phase analysis was performed following the method described by Tort et al. (2010): first, the time series of the theta oscillation phases were obtained using the Hilbert transform and the envelop of the gamma oscillation was extracted. Then, theta phase was binned (5° bins) and the mean amplitude of the gamma composite envelope was calculated on each bin. Finally, the mean amplitude was normalized by the sum of the amplitude across all bins. The histogram obtained with this method was fitted with a sine wave for each mouse in order to compute the modulation index (max-min of the sinusoidal fit) and the preferred phase of gamma oscillation (phase of the sine wave peak; see polar plots). Gamma envelops were also randomly permuted using the function *circshift* in Matlab (surrogates) to compute the mean amplitude of gamma surrogates on each bin of theta phase. To assess the statistical significance of theta/gamma modulation, we performed a Wilcoxon test between the modulation index of the raw data and the surrogates.

Spiking analysis. Spike time occurrences were determined as threshold amplitude crossings on Spike 2, and spike detection was checked for all recordings included in the analysis. Mean firing rate was computed per episode for each state and then averaged across all episodes for each cell. To assess whether a cell was significantly modulated by whisking behavior in wakefulness and/or in REM, we selected periods of active wakefulness or REM-noWh occurring 1 s before or after the whisking episode, and we then compared its firing rate across these paired episodes of Wh/aWK and RWM/REM-noWh. Only cells for which at least five paired episodes were recorded were included in this analysis (*t* test for paired data, significant if $p < 0.05$).

Bursts were defined as two or more spikes that were preceded by at least 65 ms of silence and had interspike intervals (ISIs) <8 ms. A maximal ISI of 8 ms was chosen in order to include the last spikes fired in long bursts (Urbain et al., 2019). Only cells for which >100 spikes were collected in the states of interest (NREM, REM-noWh and RWM for the study of the percentage of spikes included in bursts, NREM and REM-noWh for the comparison of bursts characteristics) were considered for this study. Cells were considered to fire in bursts in one state if the percentage of spikes included in bursts was superior to 50%. No ISI < 1 ms was observed, indicating single-unit recording. In order to illustrate the high-frequency burst activity during NREM and REM, we showed the instantaneous frequency of the thalamic cell, calculated as 1/ISI.

Spindle detection. S1-LFP spindles were observed as transient waxing and waning oscillatory events in the 10–18 Hz range (see Materials and Methods in Urbain et al., 2019). Briefly, S1-LFP spindles were detected by applying a ridge line detection on the wavelet time frequency map using a custom-written script in Python. For spindle detection during NREM, the threshold was set as three times the median power of the 10–18 Hz band excluding NREM periods. This threshold was adjusted from our previous study (threshold of 4) in order to take into account the decrease in REM spindles amplitude compared with NREM. Only oscillations spanning more than three cycles were kept for analysis. Each detected spindle was converted into a time frequency line giving for each time point: instantaneous frequency, phase, and power of the spindle. For comparison of spindles parameters between NREM and REM, only spindles in NREM episodes preceding REM were considered (in order to have the same number of NREM and REM episodes in both samples) and a minimum of five spindles in each state was required to be considered for this analysis.

Phase analysis. Phase analysis of VPM neurons firing onto S1-LFP spindles was performed following the method already used in our previous paper (Urbain et al., 2019). The phase of action potentials (APs) relative to spindles in the S1-LFP was determined by the angle of the instantaneous phase (derived from a Hilbert transformation of the S1-LFP) at the location of spikes. The trough of the spindles was defined as 0° and the peak as 180°. These two points define the reference frame, which enabled us to compare waves with different shapes and lengths. For each cell, we built phase histograms of spike timing relative to spindle troughs. Only neurons which fired at least 50 APs during spindle bouts were included in the analysis. Firing was considered to be modulated by the oscillations if $p < 0.01$ using the Rayleigh's test. To compute the grand average of modulated cells, the number of spikes per phase bin was normalized for each cell (by dividing by the total number of spikes over one spindle cycle).

Thalamic spikes were collected and aligned at their peaks to compute S1-LFP spike-triggered averages (STA). Only spikes separated by >65 ms were considered. Only cells with at least 50 spikes in both NREM and REM were kept for the analysis. S1-LFPs were collected and averaged per cell (436.7 ± 51.3 spikes per cell in NREM, 236.3 ± 28.3 spikes per cell in REM; range: 83–1,333 spikes per cell in NREM, 61–734 spikes per cell in REM), and then a grand average was calculated with the SEM. In addition, we computed the STA of the randomly permuted S1-LFP using the function *cricshift* of Matlab (surrogates). For each VPM spike, S1-LFP was permuted 100 times in the interval −0.1 to 0.2 s relative to the spike. The average surrogate STA for the cell was the average of all the permutations on all spikes. To assess the statistical significance of the STA in each state (NREM and REM), the peak value of S1-LFP and its surrogates was computed for each cell and a Wilcoxon test was performed.

For the VPM spikes distribution on the delta waves, spindles preceded by a delta event were detected by visual inspection for each cell and aligned at the spindle onset. Thalamic spike time occurrences were distributed in a peristimulus time histogram (−500 to 500 ms PSTH, 50 ms bins). Only the time windows for which the cell fired at least 10 spikes were kept for the analysis, and only cells with at least five windows (i.e., 5 delta events with at least 10 spikes) were considered.

Statistical analysis. Data analysis was performed using Spike2, Matlab, Python, and Excel software. Unless otherwise stated, results are reported as mean ± SEM. Statistical analysis was performed using Matlab. The Tukey–Kramer or the Dunn–Sidak test was chosen when a post hoc test was applied. Circular statistics was performed using the "*circular statistics toolbox*" in Matlab. Statistical tests are specified in the figure legends. The numbers of cells and mice considered for each test are provided in the main text or/and in figure legends. Additional statistical measures (such as mean, median, range) are provided in Extended Data Tables 1-1 and 3-1–5-1. Except otherwise stated, spectral power for EEG and LFP data were compared across states using Friedman or Wilcoxon tests; other data were compared across states using ANOVA for repeated measures or *t* test for paired data. Significance levels $*p < 0.05$; $**p < 0.01$; $***p < 0.001$.

Results

We performed S1-LFP associated with extra- and intracellular recordings of thalamic relay cells while simultaneously measuring the EEG and the EMG. These recordings allowed us to investigate the cortical dynamics and their thalamic correlates in REM and to compare them with those observed in wakefulness (WK) and NREM sleep in nonanesthetized head-fixed mice.

Rapid whisker movements are associated with phasic cortical activity in REM

Rapid whisker movements (RWMs) were observed during REM despite the atonia measured at the level of the neck muscles (Fig. 1), as we previously reported (Brécier et al., 2022). RWM represented on average 20%, while nonwhisking periods (REM-noWh) accounted for approximately half of the total REM duration (Fig. 1C, average across 110 episodes of REM from 32 mice); and the probability to observe RWM was significantly higher in the last two thirds of REM episodes compared with the first third (respectively, 4.3 ± 0.2, 6.4 ± 0.3, and 6.6 ± 0.4% in the first, second, and third parts of the REM; $p = 2 \times 10^{-5}$ and $p = 4 \times 10^{-5}$). Compared with free-whisking during wakefulness (Wh), RWMs were significantly faster (RWM,

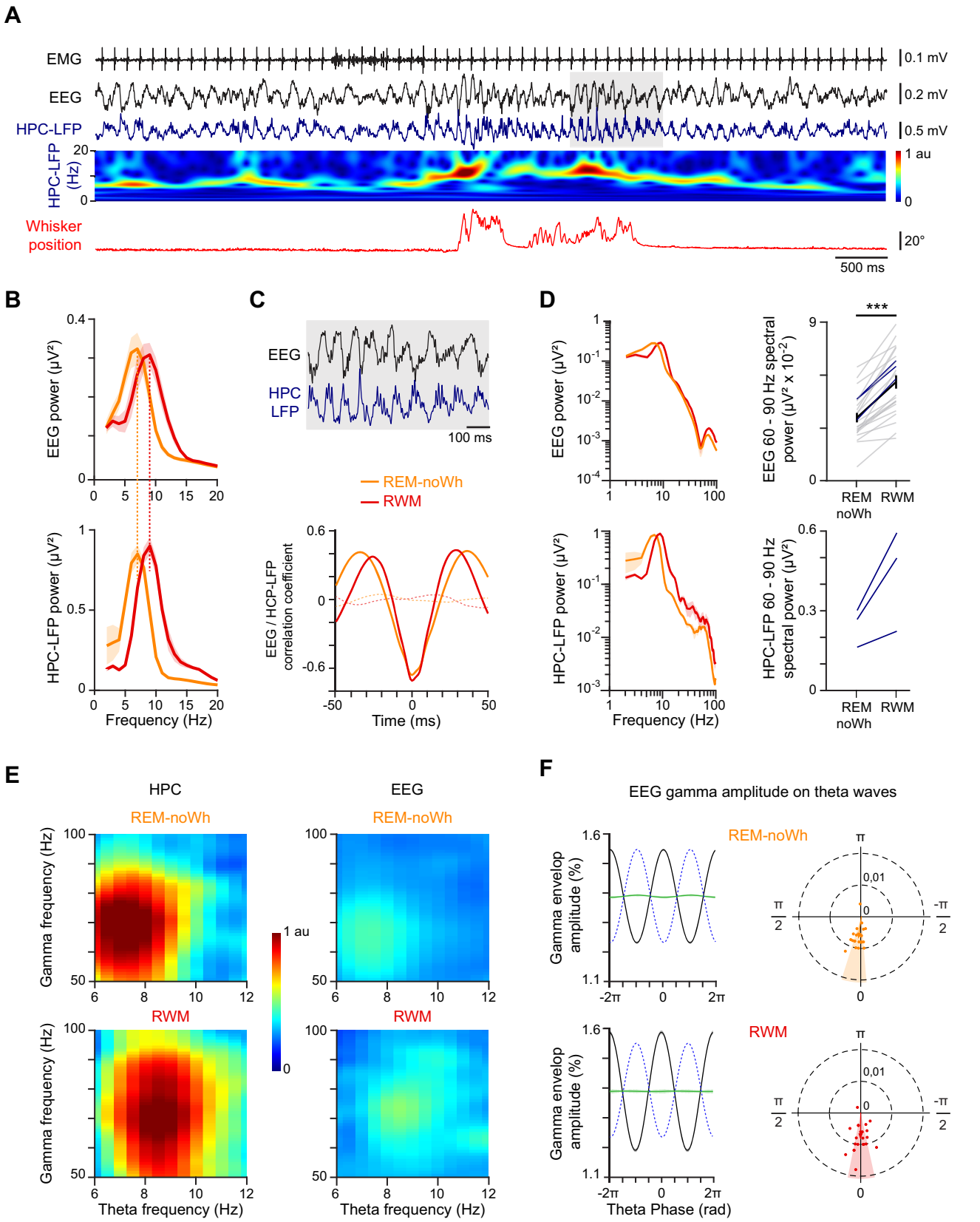

Figure 2. Hippocampal activity is highly correlated to the EEG in the theta band in REM. ***A***, Typical recording of HPC activity during and outside whisking behavior in REM. Top to bottom, Neck EMG, EEG, HPC-LFP (blue), and corresponding HPC-LFP wavelet time-frequency spectrum (color graph) and whisker position (red). ***B***, Grand average PSDs of EEG (top) and HPC-LFP (bottom) recorded on three mice across REM-noWh (orange) and RWM (red). ***C***, Top, Enlarged view of the gray box in ***A***. Bottom, Grand average cross-correlogram between EEG and HPC-LFP in REM-noWh and RWM, compared with shuffled data (dashed lines). ***D***, Left, Grand average PSD of EEG (top) and HPC-LFP (bottom) in REM-noWh and RWM displayed with a logarithmic scale. Right, Corresponding average EEG (mean ± SEM in black; Wilcoxon test) and HPC-LFP spectral power per mouse in the gamma range (60–90 Hz); blue lines correspond to the three cells for which both EEG and HPC-LFP recordings were available. ***E***, Phase-amplitude comodulograms for HPC-LFP (left) and the EEG (right) in REM-noWh (top) and RWM (bottom; see Materials and Methods).

14.0 ± 0.3 Hz vs Wh, 10.6 ± 0.2 Hz; $p = 2 \times 10^{-9}$; $n = 35$ mice) and smaller in amplitude (RWM, 34.1 ± 0.6° vs Wh, 39.2 ± 0.8°; $p = 9 \times 10^{-7}$; Fig. 1*D–F*). Whisking prominence, i.e., the amplitude of protraction/retraction cycles, was significantly lower in REM (RWM, 14.6 ± 0.2° vs Wh, 21.1 ± 0.6°; $p = 4 \times 10^{-12}$), indicating a more focal whisking than in wakefulness. RWM episodes were also significantly shorter than in wakefulness (RWM, 1.05 ± 0.04 s vs Wh, 1.53 ± 0.07 s; $p = 10^{-6}$), but with no variation in the number of cycles per episode (RWM, 12.3 ± 0.5 vs Wh, 14.2 ± 0.7; $p = 0.05$).

RWMs were associated with a significant increase in EEG theta frequency compared with tonic REM (RWM, 8.8 ± 0.1 Hz vs REM-noWh, 6.7 ± 0.1 Hz; $p = 2 \times 10^{-16}$; average across 32 mice) but with no change in theta power (Fig. 1*G*; $p = 0.98$). To examine the hippocampal activity associated with RWM, we performed LFP recordings in the CA1 area of the dorsal hippocampus (HPC; Fig. 2); in all animals (three mice), we observed that hippocampal theta oscillations show similar properties and a high correlation with the ones on the EEG. These results support the hypothesis that EEG theta rhythms mostly reflect hippocampal REM activity in mice (Bland and Whishaw, 1976; Sirota et al., 2008). RWMs were also associated with an increase in gamma activity at both the EEG and hippocampal level: gamma oscillations (60–90 Hz) power was significantly increased during RWM (Fig. 2*D*; EEG: REM-noWh, 0.036 ± 0.003 μV², RWM, 0.056 ± 0.04 μV²; $p = 3 \times 10^{-5}$), and gamma amplitude was modulated on the theta wave (Fig. 2*E,F*; Rayleigh test $p < 0.01$). Taken together, our results indicate that RWM are strongly correlated with phasic hippocampal activity during REM. We will therefore hereafter consider two substates of REM: RWM and REM-noWh, corresponding to previously reported phasic and tonic REM substates (Brankačk et al., 2012; Simor et al., 2020; Dong et al., 2022).

S1-LFP exhibits both wakefulness and NREM features in REM

We observed the presence of a high delta (2–6 Hz) power on S1-LFP during tonic REM (Fig. 3*A,B*; spectral power: 4.5 ± 0.7 μV²), which decreased significantly during RWM bouts (2.8 ± 0.5 μV²; $p = 4 \times 10^{-6}$; $n = 28$ mice). This alternation between periods with high and low delta power is reminiscent of what we previously described on S1-LFP activity during wakefulness (Urbain et al., 2015); indeed quiet wake periods (qWK), characterized by large-amplitude slow S1-LFP fluctuations in the delta range, alternated with active wake episodes, either with (Wh) or without (aWK) whisking (Fig. 3*B*; delta spectral power: qWK, 4.6 ± 0.7 μV²; Wh, 0.8 ± 0.1 μV²; aWK, 0.9 ± 0.2 μV²; qWK vs Wh, $p = 3 \times 10^{-8}$; qWK vs aWK, $p = 10^{-7}$; aWK vs Wh, $p = 0.99$). Interestingly, strong delta power during tonic REM was restricted to S1-LFP [S1-LFP: 3.3 ± 0.8 μV², M1-LFP: 1.3 ± 0.3 μV², EEG: 1.3 ± 0.2 μV²; M1 vs S1, $p = 4 \times 10^{-3}$; EEG vs S1, $p = 0.2$ (note the high theta power in the EEG); M1 vs EEG, $p = 0.5$; $n = 11$ mice] in contrast with the more global delta rhythm observed in qWK (S1-LFP, 4.0 ± 0.7 μV²; M1-LFP, 4.6 ± 0.8 μV²; EEG, 2.3 ± 0.2 μV; M1 vs S1, $p = 1.0$; EEG vs S1, $p = 0.06$; M1 vs EEG, $p = 0.1$; Fig. 3*C,D*). These results suggest that S1-LFP displays, throughout REM episodes, overall delta activity that closely mimics its wakefulness counterpart dynamics, in that delta power significantly decreases with the appearance of whisker movements in both vigilance states.

We next compared the delta band power on S1-LFP calculated in tonic REM with the one computed in NREM (Fig. 4*A,B*; REM-noWh, 4.5 ± 0.7 μV² vs NREM, 5.2 ± 0.8 μV²; $p = 0.02$; $n = 28$ mice), since delta waves are also typically observed during NREM (Amzica and Steriade, 1998; Urbain et al., 2019). On normalized spectra of S1-LFP between 2 and 20 Hz, delta power in tonic REM was significantly larger than its NREM counterpart (REM, 56.1 ± 1.3% vs NREM, 50.0 ± 1.6%; $p = 9 \times 10^{-4}$).

Strikingly however, REM S1-LFP also displayed strong sigma (10–18 Hz) power, which is a well-known hallmark of NREM spindle activity (Fig. 4*C*; REM, 1.3 ± 0.3 μV² vs NREM, 2.2 ± 0.3 μV²; $p = 2 \times 10^{-4}$; $n = 28$ mice). In order to determine whether this REM-sigma activity was subtended by spindles, we applied an algorithm that was developed during a previous study of S1-LFP in NREM (Urbain et al., 2019) to automatically detect individual spindles (Extended Data Fig. 4-1*A*; see Materials and Methods). The algorithm robustly detected spindles throughout REM, but with a significantly lower rate and density than those observed in NREM (rate: REM, 0.27 ± 0.03 vs NREM, 0.58 ± 0.02 spindles/s; $p = 10^{-11}$; density: REM, 11.7 ± 1.3 vs NREM, 39.6 ± 1.6%; $p = 10^{-14}$, $n = 37$ mice; Fig. 4*D*; Fig. 4-1*B*). Spindles were of similar frequency in REM than in NREM (REM, 12.9 ± 0.1 Hz vs NREM, 12.7 ± 0.1 Hz; $p = 0.03$; $n = 32$ mice), but of significantly shorter durations (REM, 0.42 ± 0.01 s vs NREM, 0.67 ± 0.02 s; $p = 6 \times 10^{-15}$), with a lower number of cycles per spindle (REM, 5.4 ± 0.1 vs NREM, 8.4 ± 0.3; $p = 2 \times 10^{-14}$). They occurred preferentially outside RWM (Fig. 4*E*; REM-noWh, 15.6 ± 1.6 vs RWM, 7.1 ± 1.2%; $p = 3 \times 10^{-6}$; $n = 35$ mice).

Taken together, these data indicate that REM is composed of two distinct substates with characteristics reminiscent of both wakefulness and NREM: a phasic state characterized by a cortical activation associated with RWM, similar to active wakefulness; and tonic REM, characterized by delta oscillations coupled with the appearance of spindles, closely resembling S1-LFP in NREM.

Thalamic neurons display both wakefulness and NREM activity patterns during REM

In order to further probe the REM substate dynamics observed on S1-LFP, we recorded the firing activity and membrane potential (Vm) of somatosensory relay cells in the ventroposterior medial (VPM) thalamus. VPM neurons mean firing rate increased significantly during active compared with quiet wakefulness and further increased during whisking (Fig. 5*A,B*; Wh, 20.3 ± 2.3 spikes/s, aWK, 12.1 ± 2.0 spikes/s and qWK, 5.6 ± 1.4 spikes/s; Wh vs aWK, $p = 10^{-6}$; Wh vs qWK, 9×10^{-10}; aWK vs qWK, 9×10^{-5}; $n = 32$ cells), in agreement with our previous study (Urbain et al., 2015). Those same neurons exhibited a similar significant increase in mean firing rate associated with RWM during REM (24.8 ± 3.4 vs REM-noWh, 16.2 ± 2.0 spikes/s; $p = 5 \times 10^{-4}$). VPM cells were as active during RWM as in wake whisking (Fig. 5*B*; $p = 0.07$, $n = 35$ cells). Moreover, approximately half of the cells recorded in both wakefulness and REM

←

Warm colors illustrate that the amplitude of gamma oscillations is modulated with the theta wave. ***F***, Left, Distribution of the mean EEG gamma envelop amplitude (black line) on the EEG theta waves (dotted blue line) in REM-noWh (top) and RWM (bottom). Average of shuffled gamma envelops is represented in green. Right, Gamma oscillation maximum amplitude preferred phases and modulation amplitudes on theta waves for the EEG, in REM-noWh and RWM. Colored areas represent the confidence interval at 95%. ***B–F***, REM-noWh data are illustrated in orange and RWM data in red. ***C–F***, HPC, $n = 3$ mice; EEG, $n = 23$ mice. See Extended Data Table 1-1 for additional statistical measures.

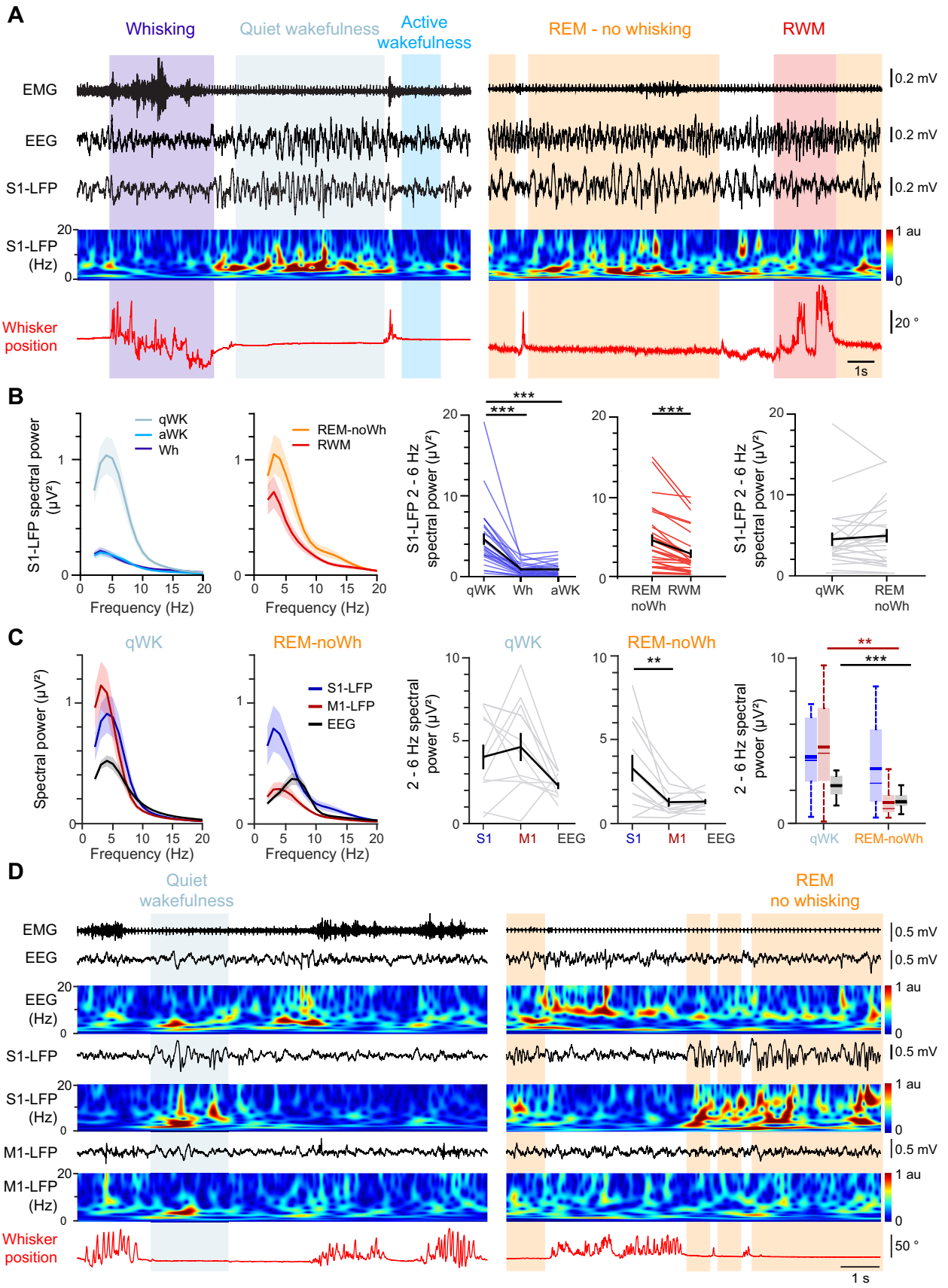

Figure 3. S1-LFP exhibits typical wakefulness features in REM. ***A***, S1-LFP activity during wakefulness (left) and REM (right). Top to bottom, Neck EMG, EEG, S1-LFP, corresponding S1-LFP wavelet time-frequency FFT (color graph), and whisker position (in red). ***B***, Left two panels, Grand average PSDs of S1-LFP in the different substates of wakefulness (blue) and REM (red). Middle two panels, Corresponding average S1-LFP spectral power in the delta range (2–6 Hz). Right, No significant difference in the delta spectral power was observed between qWK and REM-noWh. In black, mean ± SEM; $n = 28$ mice. ***C***, Left two panels, Grand average PSD of S1-LFP (blue), M1-LFP (red), and EEG (black) in qWK and REM-noWh. Middle two panels, Corresponding average

(17/32) significantly increased their firing rate during whisking in wakefulness, and 70% of them were similarly modulated by RWM (Fig. 5*C*). Less than 10% were modulated in RWM only. Self-generated whisker movements may therefore drive thalamic activity through direct sensory activation in REM, as previously described in wakefulness (Fee et al., 1997; Urbain et al., 2015).

While all recorded VPM cells fired, as expected, high-frequency bursts of spikes during NREM, 43% (16/37) of them conserved this firing pattern during REM and only switched to a tonic firing mode during RWM (Fig. 5*D*,*E*; NREM, 82.1 ± 3.0% of spikes included in bursts; REM-noWh, 70.3 ± 2.8%; RWM, 25.4 ± 5.3%; REM-noWh vs NREM, $p = 0.2$; RWM vs NREM, $p = 9 \times 10^{-7}$; REM-noWh vs RWM, $p = 2 \times 10^{-3}$; $n = 13$ cells). The remaining 57% of cells switched to a tonic firing mode at the initiation of REM (Fig. 5*D*,*F*; NREM, 69.0 ± 6.7% of spikes included in bursts; REM-noWh, 8.7 ± 2.3%; RWM, 2.5 ± 0.5%; REM-noWh vs NREM, $p = 3 \times 10^{-3}$, RWM vs NREM, $p = 4 \times 10^{-5}$, REM-noWh vs RWM, $p = 0.6$; $n = 16$ cells) and maintained this firing mode throughout REM episodes. Both populations displayed a similar significant firing rate modulation on RWM; however, no specific relationship was observed between burst firing patterns in REM and firing rates on RWM (Fig. 5*G*). Bursts of spikes in REM displayed the same characteristics as the NREM thalamic bursts (Domich et al., 1986; Urbain et al., 2019), i.e., same mean ISI (Fig. 5*H*; 2.4 ± 0.0 ms in both NREM and REM; $p = 0.2$; $n = 16$ cells) and same dynamics of ISI durations and spike amplitudes within a burst (Extended Data Fig. 5-1*A*,*B*). They occurred at the same rate than during NREM (Extended Data Fig. 5-1*C*; REM, 1.2 ± 0.5 vs NREM, 1.1 ± 0.4 burst/s; $p = 0.7$), despite a significant increase in burst duration (REM, 8.0 ± 0.1 ms vs NREM, 6.0 ± 0.1 ms; $p = 10^{-7}$), with a higher number of spikes per burst (REM, 4.3 ± 0.0 vs NREM, 3.5 ± 0.0 spikes; $p = 7 \times 10^{-6}$).

Remarkably, our intracellular recordings revealed the presence of spindle oscillations on the membrane potential (Vm) of a subset of VPM neurons (3/6) in NREM as well as in REM (Fig. 6*A*). Thalamic Vm spindles density decreased in REM compared with NREM, concomitantly with the observed decrease at the level of S1-LFP (NREM, 35% vs REM, 5%; $n = 3$ cells). Interestingly, we observed that VPM-Vm was more depolarized during REM than NREM (Fig. 6*B*,*C*; 4.5 mV more depolarized on average; $n = 3$ cells for which our intracellular recordings were stable across the entire sleep-wake cycle), in agreement with a previous study in cats (Hirsch et al., 1983).

Together, our data show a highly dynamic modulation of thalamic cells firing during REM: a tonic activity during RWM, reminiscent of whisking in wakefulness, as well as high-frequency bursts, which closely resemble their NREM firing pattern.

Thalamocortical coupling is maintained during REM in the somatosensory pathway

High-frequency VPM thalamic bursts occur preferentially on the rising phase of cortical spindle cycles and were therefore believed to be directly involved in spreading spindles generated within the thalamus to the cortex during NREM (Halassa et al., 2011; Urbain et al., 2019). To obtain further insight into the thalamic and cortical coupling occurring during REM, we analyzed the timing of VPM spikes relative to S1-spindle cycles in REM. We found that fewer VPM spikes were phase locked in REM compared with NREM (17/24 vs 22/24, respectively; Rayleigh test $p < 0.01$; Fig. 7*A*–*C*). However when the neurons were phase locked, they showed similar phase preference in both states (NREM, 83 ± 14° before the spindle trough; REM, 81 ± 11°; $n = 17$ cells). Reciprocally, VPM population spike-triggered averaging (STA) on S1-LFP revealed a peak, with a lag of <20 ms after thalamic spiking in both NREM and REM (Fig. 7*D*; REM, 19 ms vs NREM, 15 ms).

In addition, we observed that spindles in S1 were often preceded by a delta wave during REM, as previously reported during NREM (Urbain et al., 2019). Since these delta events in NREM were associated with a decrease in VPM firing rates, we examined the firing rate of VPM cells recorded extracellularly relative to S1-spindles preceded by delta waves during REM. We computed PSTHs of VPM spikes aligned to spindle oscillation onset and found a significant decrease in VPM discharge during delta events (Fig. 7*E*; −200 to −50 ms, 11.4 ± 1.7 Hz vs baseline, 20.6 ± 1.7 Hz; $p = 2 \times 10^{-5}$; $n = 22$ cells). At the subthreshold level, these REM delta events were accompanied by a significant hyperpolarization of VPM-Vm (Fig. 7*F*; −200 to −50 ms period: −0.4 ± 0.1 mV; $p = 0.03$; $n = 6$ cells). Taken together, these results suggest a strong thalamocortical oscillatory coupling during REM, with marked similarities to NREM coupling.

Discussion

We report a transient cortical activation in S1-LFP associated with RWMs alternating with a high-amplitude and low-frequency activity during REM, reminiscent of the S1-LFP activity observed in wakefulness and NREM respectively. By focusing on the lemniscal pathway of the well-defined mouse whisker system, we applied cross-correlations together with phase and time-frequency analysis to extra- and intracellular recordings performed in the thalamic VPM cells and the corresponding barrel somatosensory cortex and were able to demonstrate that some spindle activity propagating from the VPM thalamus to barrel cortex is maintained during REM. We described RWMs during REM in adult mice (observed in newborn rats by Tiriac et al., 2012); this is of particular interest regarding REM sleep function considering that mice are nocturnal animals and extensively use their whiskers to explore their environment. RWMs are faster and more foveal than those occurring during wakefulness (Fig. 1), suggesting either that foveal whisking is more represented in REM or that RWMs have different kinetics than wake whisking, as reported for eye movement properties in REM versus wakefulness (Vanni-Mercier et al., 1994; Sprenger et al., 2010; Sánchez-López and Escudero, 2011; Andrillon et al., 2015).

During RWMs, we observed a cortical activation on S1-LFP similar to the one during whisking behavior in wakefulness; this activity alternated with a tonic state resembling NREM outside of these phasic events. However, both substates occurred during REM sleep episodes, clearly identified through neck muscle atonia and prominent EEG theta activity (Fig. 1). RWMs were

←

S1-LFP, M1-LFP and EEG spectral power per mouse in the delta range in qWK and REM-noWh (in black, mean ± SEM). Right, Comparison of grand average S1-LFP (blue), M1-LFP (red), and EEG (black) spectral powers in the delta range between qWK and REM-noWh. Boxplots indicate mean (thick line), median (thin line), and interquartile range; $n = 11$ mice. ***D***, Cortical activity during wakefulness and REM. Top to bottom, Neck EMG, EEG, S1-LFP, M1-LFP, and their corresponding wavelet time-frequency FFTs (color graphs) and associated whisker position (in red). ***B***, ***C***, See Extended Data Table 3-1 for additional statistical measures.

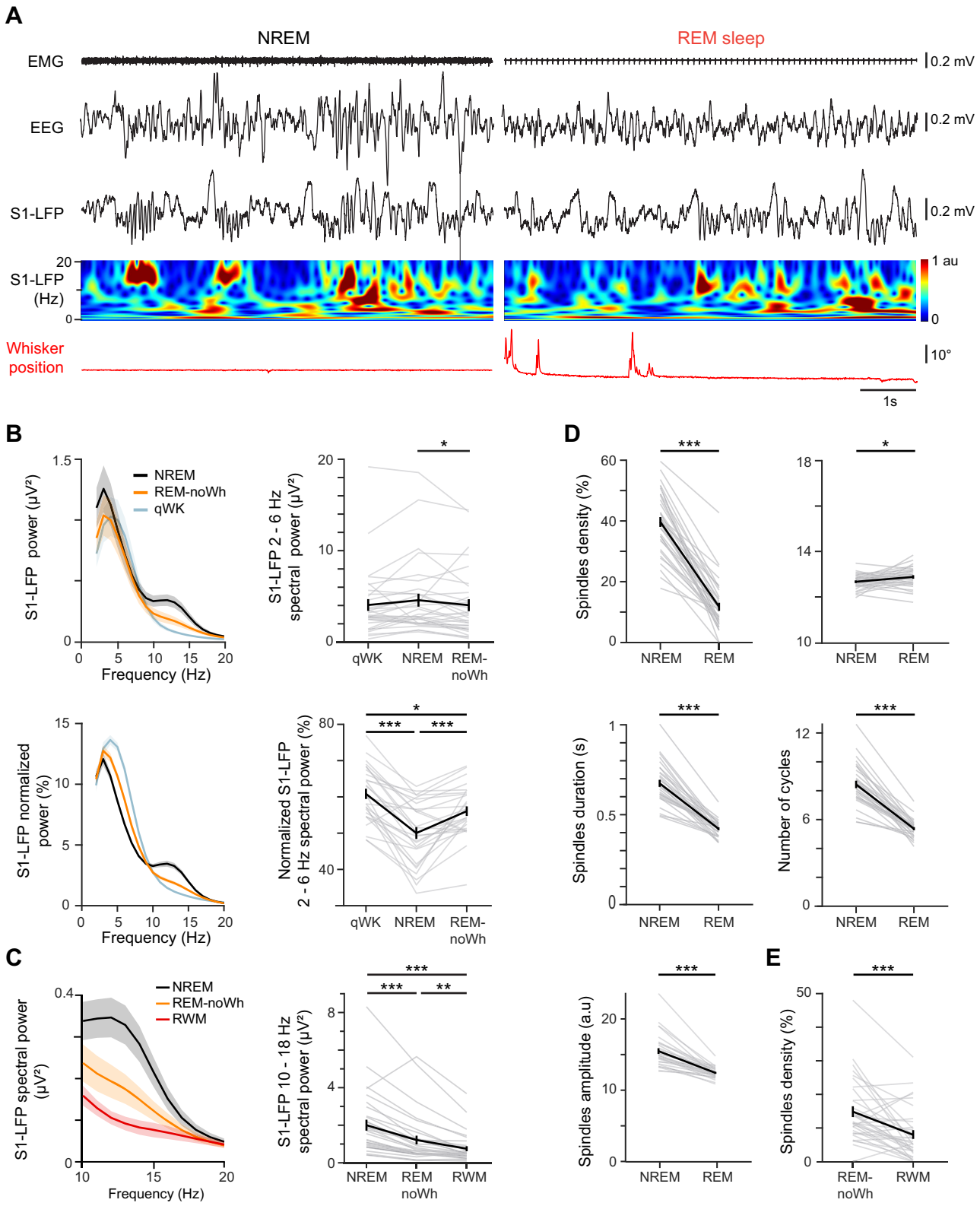

Figure 4. S1-LFP exhibits typical NREM spindle oscillations in REM. ***A***, S1-LFP activity during NREM and REM. Top to bottom, Neck EMG, EEG, S1-LFP, corresponding S1-LFP wavelet time-frequency FFT (color graph) and whisker position (in red). ***B***, Top, Grand average PSD of S1-LFP in NREM (black), REM-noWh (orange), and qWK (gray) and corresponding spectral power in the delta range. Bottom, Distribution of grand average spectral power (normalized PSD) of S1-LFP in NREM, REM-noWh, and qWK and corresponding mean distribution per mouse in the delta range ($n = 28$ mice). ***C***, Left, Grand average PSD of S1-LFP in the sigma range (10–18 Hz) in NREM (black), REM-noWh (orange), and RWM (red). Right, Corresponding average S1-LFP spectral power per mouse ($n = 28$ mice). ***D***, Average spindle parameters per mouse in NREM and REM: density ($n = 37$ mice), frequency, duration, number of cycles and relative amplitude (see Materials and Methods and Extended Data Fig. 4-1; $n = 32$ mice). ***E***, Average spindle density calculated in REM-noWh and RWM ($n = 35$ mice). The solid line represents the mean ± SEM; data were compared across states using Friedman (***B***,***C***) and Wilcoxon tests (***D***,***E***); see Extended Data Table 4-1 for additional statistical measures.

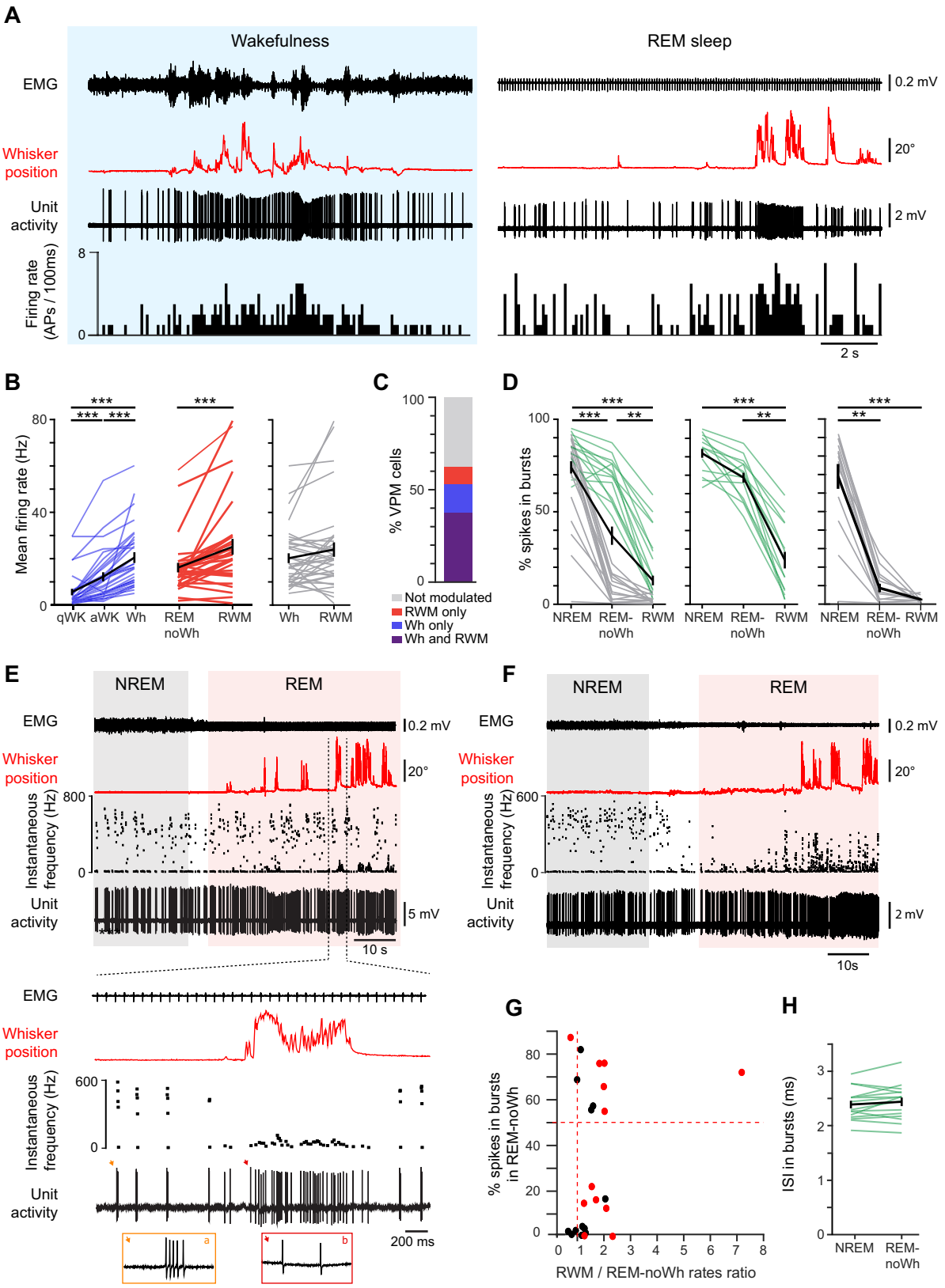

Figure 5. Thalamic neurons activity in REM exhibits both wakefulness and NREM patterns. ***A***, Activity of a typical VPM cell during wakefulness (left) and REM (right). Top to bottom, Neck EMG, whisker position (in red), VPM neuron unit activity, and firing rate (100 ms bins). ***B***, Left, Mean firing rate of VPM neurons in wakefulness (blue) and REM (red; $n = 32$ cells recorded in all five states). Right, Comparison between whisking mean firing rates in wakefulness and REM ($n = 35$ cells in Wh and RWM). ***C***, Percentage of whisking-modulated VPM cells ($n = 32$ cells). ***D***, Percentage of spikes in bursts in NREM, REM-noWh and RWM for all cells (left, $n = 29$ recorded in all three states), for subpopulations of VPM neurons that fired bursts of spikes (green; middle; $n = 13$) or tonically (gray; right; $n = 16$) in REM-noWh. ***E***, Top, Unit activity of an example VPM neuron showing bursting activity across NREM and REM and associated EMG (top trace), whisker position (red trace), and the instantaneous frequency (middle trace, 1/ISI) showing that high-frequency bursts were observed in both NREM and REM (Extended Data Fig. 5-1 and Extended Data Table 5-1), but outside of whisker movements. Bottom, Enlarged view of the boxed area with 20 ms insets showing a burst of spikes in REM-noWh or a single-spike

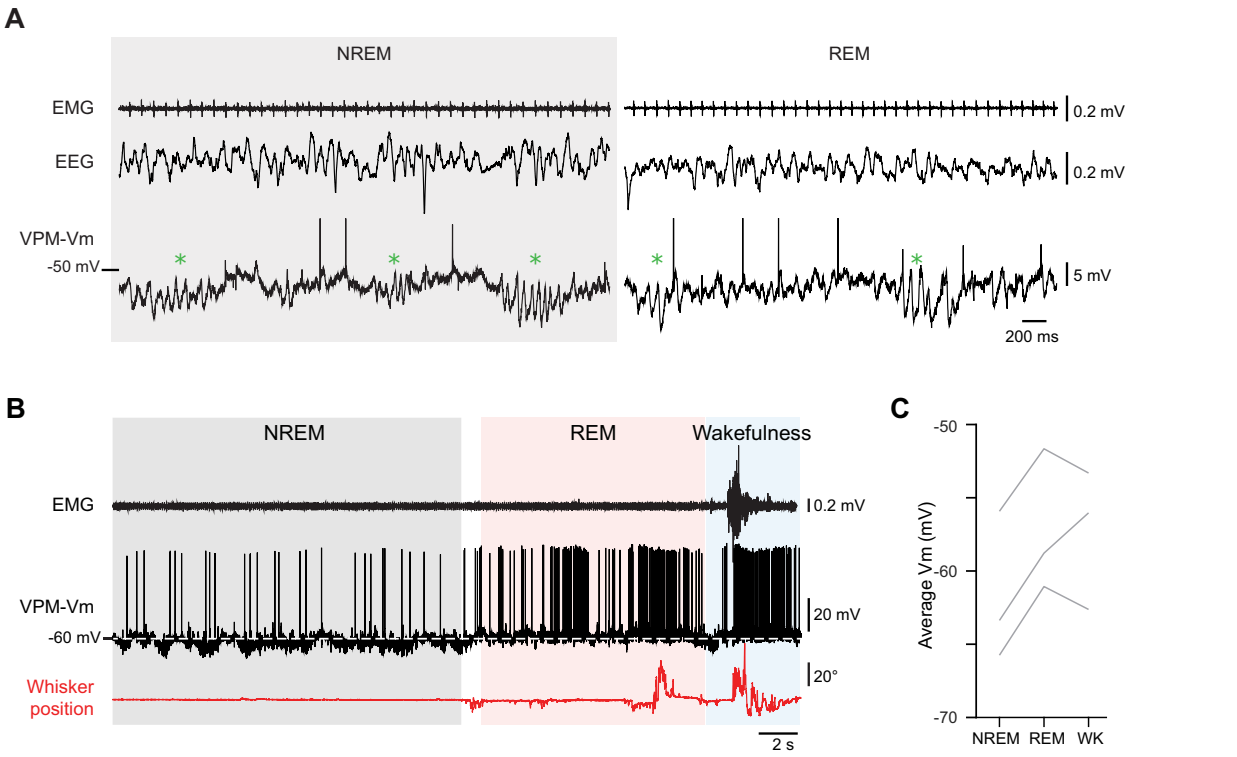

Figure 6. Thalamic membrane potential activity displays both typical wakefulness and NREM features. ***A***, Example of the membrane potential (Vm) of a VPM cell recorded in NREM (left) and REM (right), together with EMG (top) and EEG (middle). Oscillations in the spindle frequency range (green stars) can be observed in both states. Spikes are truncated. ***B***, Membrane potential of a typical VPM cell (Vm-VPM), and the associated EMG (top trace) and whisker position (in red) across NREM, REM and wakefulness. ***C***, Grand average of VPM-Vm in NREM, subsequent REM and wakefulness ($n = 3$ cells).

associated with an increase in both theta frequency and gamma power measured on the EEG and HPC-LFP, as previously reported for REMs in humans and rodents (Montgomery et al., 2008; Brankačk et al., 2012; Simor et al., 2016). A higher synchrony between theta and gamma activity in phasic compared with tonic REM may allow the opening of short windows of communication between the HPC and the cortex, suggesting a role for phasic REM sleep in hippocampocortical memory consolidation (De Almeida-Filho et al., 2021).

LFP activity in S1 was highly dynamic across phasic and tonic REM substates. Notably, a strong LFP delta power was present during tonic REM, but restricted to S1 (Fig. 3), in contrast to the high coherence of S1- and M1-LFP activity for delta oscillations reported in quiet wakefulness (Funk et al., 2016; Baird et al., 2018). Since functional coupling between distributed cortical areas through synchronized activities is thought to play an important role for many cognitive processes, including attention and decision-making, and supports consciousness (Varela et al., 2001; Buzsáki and Draguhn, 2004; Tononi and Massimini, 2008), especially in the delta-theta band (Bourdillon et al., 2020), our findings suggest that cortical sensory networks process information in a more segregated manner during REM, potentially subtending the lack of consciousness during REM and dreaming.

We further uncovered the unexpected presence of spindle oscillations during tonic REM (Fig. 4), while they are typically exclusively associated with NREM. Given the thalamic origin of cortical NREM spindle activity (for review, McCormick and Bal, 1997; Lüthi, 2014), we looked for thalamic neuronal correlates of REM spindles observed on S1-LFP and found that a subset of VPM cells (16/37) maintained high-frequency bursting activity while the animal was in REM, a firing mode typically associated with NREM. These VPM bursts of spikes displayed the same properties as those observed during NREM (Fig. 5), including preferential firing on the rising phase of cortical spindle cycles (Urbain et al., 2019). These results suggest that the thalamocortical mechanisms generating spindle activity during NREM are maintained during REM. However, we observed a depolarization of VPM-Vm in REM compared with Vm in NREM, as previously shown by Hirsch et al. (1983) in cats, the only paper in the literature to our knowledge reporting intracellular recordings in thalamic cells during REM. This finding fits well with our observation that approximately half of VPM cells switch from a bursting activity in NREM to a tonic firing in REM but raises the question: how can a subset of thalamic VPM cells promote spindle activity during REM if they are depolarized? It was previously shown that the activation of only a small fraction of the T-type channel population is required to

←

firing in RWM. ***F***, Same as ***E*** for a VPM neuron which switched from a bursting firing in NREM to a tonic discharge in REM. ***G***, For each cell, the percentage of spikes in bursts in REM-noWh is plotted against the ratio of its mean firing rate in RWM over its mean firing rate in REM-noWh ($n = 24$ cells). Red dots indicate cells whose firing rate was significantly modulated during RWM (see Materials and Methods). ***H***, Mean duration of ISIs within bursts ($n = 16$ cells exhibiting bursts in REM-noWh). ***B***, ***D***, ***H***, Black line, mean ± SEM; data were compared across states using ANOVA for repeated measures or *t* test for paired data.

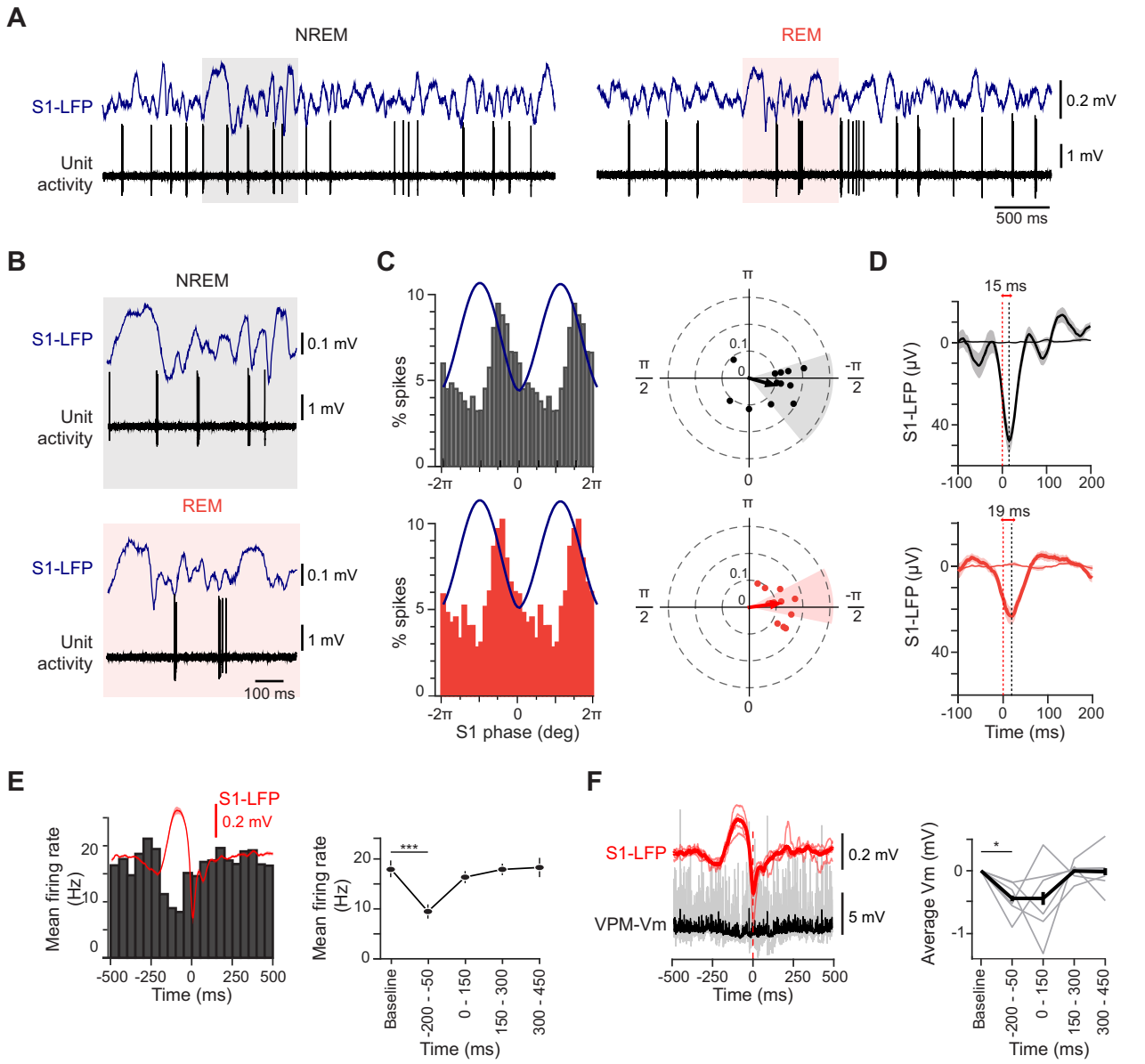

Figure 7. Thalamocortical dynamics during NREM and REM. ***A***, VPM unit activity and S1-LFP during spindle oscillations in NREM (left) and REM (right). ***B***, Enlarged view of the colored areas in ***A*** corresponding to a spindle oscillation in S1-LFP in NREM (top) and REM (bottom). ***C***, Left, Grand average spike distribution of VPM cells on S1-LFP spindle cycles (in blue; 18 bins/cycle) in NREM (top) and REM (bottom). Right, Corresponding spike firing preferred phases and modulation amplitudes on spindle cycles for modulated VPM cells. Only cells that were modulated during S1-LFP spindle cycles in both NREM and REM were considered ($p < 0.01$ Raleigh test; $n = 17$ cells). ***D***, S1-LFP grand average (mean ± SEM) triggered on VPM spikes occurring during NREM (top) or REM (bottom; $n = 20$ cells; thin lines, surrogates). ***E***, Spindles preceded by a delta wave occurring in REM were detected on S1-LFP and aligned on the spindle onset. Extracellular spike time occurrences were collected for VPM cells ($n = 22$), PSTHs were computed, and a grand average was calculated (left; 50 ms bins; $n = 22$ cells); the corresponding grand average S1-LFP delta oscillations is superimposed in red and the grand average firing rates (mean ± SEM) is illustrated to the right. ***F***, Left, S1-LFP and corresponding normalized Vm population averages for VPM cells ($n = 6$) aligned on cortical spindles onset. Right, Average normalized median Vm (150 ms bins) for these VPM cells (Black, mean ± SEM). The baseline Vm (−500 to −300 ms before S1-spindles onset) was subtracted to get the normalized data). Data from each bin were compared with baseline using a *t* test for paired data (***E***) or a Wilcoxon test (***F***). ***A–D***, NREM in black, REM in red.

generate robust calcium potentials in the ventrobasal thalamic nuclei in vitro, suggesting that high-frequency bursts of APs can actually be evoked at depolarized potentials, when the vast majority of T-type channels are inactivated (Dreyfus et al., 2010). Indeed, while Vm was on average more depolarized during REM, we observed subthreshold oscillations in the spindle frequency range in a subset of VPM cells. Therefore, a more depolarized VPM-Vm would not prevent VPM cells from being enrolled by the thalamic reticular nucleus and, in turn, from entraining cortical spindle oscillations. The latter have been shown to fire in bursts with rhythmic interburst intervals during REM at the same spindle frequency range as in NREM in freely moving rats (Marks and Roffwarg, 1993), further supporting our observations that spindles can be generated during REM. A more depolarized VPM-Vm in REM may however explain the shorter duration of the spindles observed in REM than the ones observed in NREM. Since cortical spindles and hippocampal sharp wave ripples are strongly coupled during NREM sleep (Sirota et al., 2003), our finding that spindle bouts also occur in REM, a state during which ripples are thought to be absent, raises the interesting question about what could be the function of these spindle bouts. It would be of particular interest to correlate these spindle

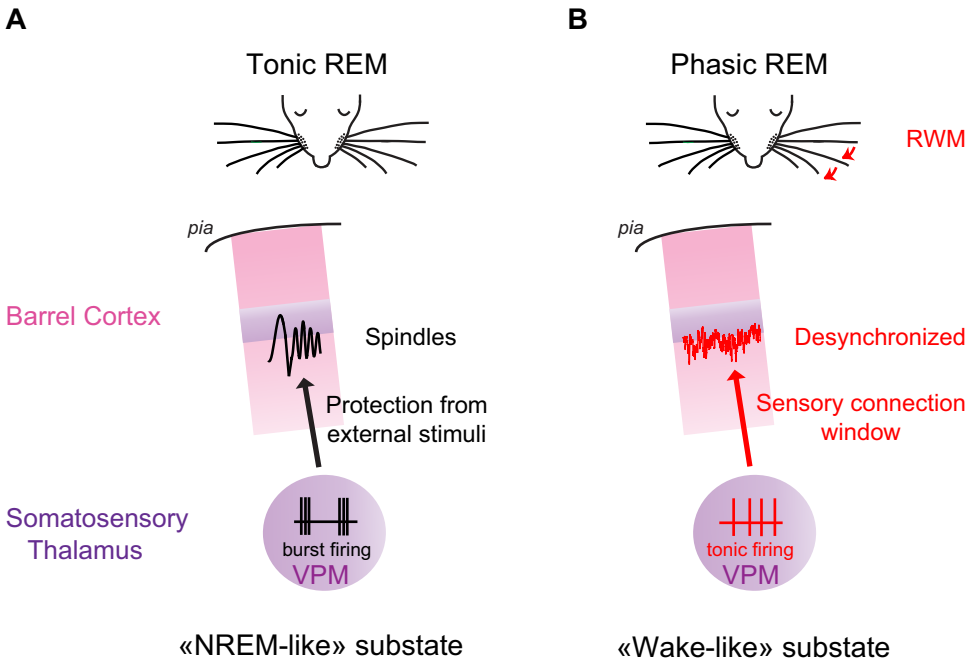

Figure 8. Schematic of differential thalamocortical dynamics during tonic and phasic states of REM. ***A***, During tonic REM, spindle bouts originating in the somatosensory thalamus spread to the barrel cortex and thalamic neurons fire high-frequency bursts, which may prevent efficient transfer of sensory information to the cortex. The system is in a NREM-like substate. ***B***, During phasic REM bouts, when whisker movements are observed, S1-LFP is desynchronized and thalamic neurons fire tonically, potentially allowing transmission of sensory information to the cortex. The system is in a wake-like substate.

bouts with increased amygdalar activation, as REM-rich sleep supports the consolidation of emotional memory (reviewed in Genzel et al., 2015; Rosier et al., 2018).

We report here that S1-LFP and neuronal activity in its corresponding thalamic nucleus display unambiguous hallmarks of NREM during tonic REM, opening new avenue on the function of REM sleep. NREM spindles were shown to elevate arousal threshold and protect the sleeper's brain from external stimuli (Wimmer et al., 2012). While the same mechanism is likely to take place during REM spindle bouts, ongoing tonic firing activity in half of VPM neurons (Fig. 5) may set the thalamocortical network at an "activatable state" level, rapidly allowing sensory transmission to resume during phasic episodes of RWM (Fig. 8). In addition, the depolarization of the membrane potential of VPM cells in REM might facilitate sensory transmission, as we showed that the firing rate of 47% of VPM neurons was significantly modulated on RWM (Fig. 5C). Notably, all the recorded VPM neurons exhibited tonic single-spike firing during RWM. Indeed, a recent study provided evidence in human of transient windows of sensory connection with the outside world during which external information can be processed in REM (Türker et al., 2023). Increased cholinergic activity in S1 may further act to suppress delta cortical activity during RWM (Nazari et al., 2023), as reported during whisking in wakefulness (Eggermann et al., 2014). Alternatively, delta waves were described to support an activity-dependent process that can weaken reactivation of memory traces and promote forgetting (Kim et al., 2019).

Tonic and phasic REM sleep may play different roles in information processing (Brankačk et al., 2012; Koroma et al., 2020). Why the brain triggers RWM during sleep and what it does with its associated tactile feedbacks remain a mystery. RWM, reminiscent in rodents of exploratory behavior in wakefulness, could be equated to other highly structured movements described in mammals during REM (Leclair-Visonneau et al., 2010; Blumberg et al., 2013) or to the rapid changes in skin patterning and texture recently described in octopus (Pophale et al., 2023). These behaviors all suggest a phasic expression during sleep of biologically and ethologically meaningful motor sequences, and they were proposed to reflect globally orchestrated representations of virtual navigation (Soh et al., 1992; Leclair-Visonneau et al., 2010; Senzai and Scanziani, 2022).

In summary, our findings show that at the level of the sensory thalamus and barrel cortex, REM sleep is not a homogeneous sleep state but rather consists of a mixture of NREM-like tonic periods interspersed with wake-like activity during phasic RWM. The NREM-like activity could potentially reduce transmission of bottom-up sensory information, thus contributing to the brain disconnection from the outside world (Funk et al., 2016; Baird et al., 2018), while thalamocortical activation, paired with higher synchrony between theta and gamma activity during RWM, could facilitate internal sensory experiences.

References

Amzica F, Steriade M (1998) Cellular substrates and laminar profile of sleep K-complex. Neuroscience 82:671–686.

Andrillon T, Nir Y, Cirelli C, Tononi G, Fried I (2015) Single-neuron activity and eye movements during human REM sleep and awake vision. Nat Commun 6:7884.

Aserinsky E, Kleitman N (1953) Regularly occurring periods of eye motility, and concomitant phenomena, during sleep. Science 118:273–274.

Baird B, Castelnovo A, Riedner BA, Lutz A, Ferrarelli F, Boly M, Davidson RJ, Tononi G (2018) Human rapid eye movement sleep shows local increases in low-frequency oscillations and global decreases in high-frequency oscillations compared to resting wakefulness. eNeuro 5:ENEURO.0293-18.2018.

Bernardi G, Betta M, Ricciardi E, Pietrini P, Tononi G, Siclari F (2019) Regional delta waves in human rapid eye movement sleep. J Neurosci 39:2686–2697.

Bland BH, Whishaw IQ (1976) Generators and topography of hippocampal theta (RSA) in the anaesthetized and freely moving rat. Brain Res 118: 259–280.

Blumberg MS, Coleman CM, Gerth AI, McMurray B (2013) Spatiotemporal structure of REM sleep twitching reveals developmental origins of motor synergies. Curr Biol 23:2100–2109.

Bourdillon P, Hermann B, Guénot M, Bastuji H, Isnard J, King J-R, Sitt J, Naccache L (2020) Brain-scale cortico-cortical functional connectivity in the delta-theta band is a robust signature of conscious states: an intracranial and scalp EEG study. Sci Rep 10:14037.

Boyce R, Glasgow SD, Williams S, Adamantidis A (2016) Causal evidence for the role of REM sleep theta rhythm in contextual memory consolidation. Science 352:812–816.

Brankačk J, Scheffzük C, Kukushka VI, Vyssotski AL, Tort ABL, Draguhn A (2012) Distinct features of fast oscillations in phasic and tonic rapid eye movement sleep: cross-frequency coupling in REM sleep. J Sleep Res 21:630–633.

Brécier A, Borel M, Urbain N, Gentet LJ (2022) Vigilance and behavioral state-dependent modulation of cortical neuronal activity throughout the sleep/wake cycle. J Neurosci 42:4852–4866.

Bueno-Junior LS, Ruckstuhl MS, Lim MM, Watson BO (2023) The temporal structure of REM sleep shows minute-scale fluctuations across brain and body in mice and humans. Proc Natl Acad Sci U S A 120:e2213438120.

Buzsáki G, Draguhn A (2004) Neuronal oscillations in cortical networks. Science 304:1926–1929.

Corsi-Cabrera M, Velasco F, Del Río-Portilla Y, Armony JL, Trejo-Martínez D, Guevara MA, Velasco AL (2016) Human amygdala activation during rapid eye movements of rapid eye movement sleep: an intracranial study. J Sleep Res 25:576–582.

De Almeida-Filho DG, Koike BDV, Billwiller F, Farias KS, de Sales IRP, Luppi P-H, Ribeiro S, Queiroz CM (2021) Hippocampus-retrosplenial cortex interaction is increased during phasic REM and contributes to memory consolidation. Sci Rep 11:13078.

Dement W (1958) The occurence of low voltage, fast, electroencephalogram patterns during behavioral sleep in the cat. Electroencephalogr Clin Neurophysiol 10:291–296.

Domich L, Oakson G, Steriade M (1986) Thalamic burst patterns in the naturally sleeping cat: a comparison between cortically projecting and reticularis neurones. J Physiol 379:429–449.

Dong Y, Li J, Zhou M, Du Y, Liu D (2022) Cortical regulation of two-stage rapid eye movement sleep. Nat Neurosci 25:1675–1682.

Dreyfus FM, Tscherter A, Errington AC, Renger JJ, Shin H-S, Uebele VN, Crunelli V, Lambert RC, Leresche N (2010) Selective t-type calcium channel block in thalamic neurons reveals channel redundancy and physiological impact of $I_{Twindow}$. J Neurosci 30:99–109.

Eggermann E, Kremer Y, Crochet S, Petersen CCH (2014) Cholinergic signals in mouse barrel cortex during active whisker sensing. Cell Rep 9:1654–1660.

Fee MS, Mitra PP, Kleinfeld D (1997) Central versus peripheral determinants of patterned spike activity in rat vibrissa cortex during whisking. J Neurophysiol 78:1144–1149.

Fernandez LMJ, Comte J-C, Le Merre P, Lin J-S, Salin P-A, Crochet S (2017) Highly dynamic spatiotemporal organization of low-frequency activities during behavioral states in the mouse cerebral cortex. Cereb Cortex 27:5444–5462.

Funk CM, Honjoh S, Rodriguez AV, Cirelli C, Tononi G (2016) Local slow waves in superficial layers of primary cortical areas during REM sleep. Curr Biol 26:396–403.

Genzel L, Spoormaker VI, Konrad BN, Dresler M (2015) The role of rapid eye movement sleep for amygdala-related memory processing. Neurobiol Learn Mem 122:110–121.

Halassa MM, Siegle JH, Ritt JT, Ting JT, Feng G, Moore CI (2011) Selective optical drive of thalamic reticular nucleus generates thalamic bursts and cortical spindles. Nat Neurosci 14:1118–1120.

Hirsch JC, Fourment A, Marc ME (1983) Sleep-related variations of membrane potential in the lateral geniculate body relay neurons of the cat. Brain Res 259:308–312.

Jouvet M, Michel F, Courjon J (1959) On a stage of rapid cerebral electrical activity in the course of physiological sleep. C R Seances Soc Biol Fil 153:1024–1028.

Karashima A, Nakao M, Katayama N, Honda K (2005) Instantaneous acceleration and amplification of hippocampal theta wave coincident with phasic pontine activities during REM sleep. Brain Res 1051:50–56.

Kim J, Gulati T, Ganguly K (2019) Competing roles of slow oscillations and delta waves in memory consolidation versus forgetting. Cell 179:514–526.

Koroma M, Lacaux C, Andrillon T, Legendre G, Léger D, Kouider S (2020) Sleepers selectively suppress informative inputs during rapid eye movements. Curr Biol 30:2411–2417.

Lambert I, Roehri N, Fayerstein J, Giusiano B, Colombet B, Bénar C-G, Bartolomei F (2022) Cortico-cortical and thalamo-cortical connectivity during non-REM and REM sleep: insights from intracranial recordings in humans. Clin Neurophysiol 143:84–94.

Leclair-Visonneau L, Oudiette D, Gaymard B, Leu-Semenescu S, Arnulf I (2010) Do the eyes scan dream images during rapid eye movement sleep? Evidence from the rapid eye movement sleep behaviour disorder model. Brain 133:1737–1746.

Lefort S, Tomm C, Floyd Sarria J-C, Petersen CCH (2009) The excitatory neuronal network of the C2 barrel column in mouse primary somatosensory cortex. Neuron 61:301–316.

Lüthi A (2014) Sleep spindles: where they come from, what they do. Neuroscientist 20:243–256.

Maingret N, Girardeau G, Todorova R, Goutierre M, Zugaro M (2016) Hippocampo-cortical coupling mediates memory consolidation during sleep. Nat Neurosci 19:959–964.

Maquet P, Péters J-M, Aerts J, Delfiore G, Degueldre C, Luxen A, Franck G (1996) Functional neuroanatomy of human rapid-eye-movement sleep and dreaming. Nature 383:163–166.

Marks GA, Roffwarg HP (1993) Spontaneous activity in the thalamic reticular nucleus during the sleep/wake cycle of the freely-moving rat. Brain Res 623:241–248.

McCormick DA, Bal T (1997) Sleep and arousal: thalamocortical mechanisms. Annu Rev Neurosci 20:185–215.

Meyer G, Carponcy J, Salin PA, Comte JC (2018) Differential recordings of local field potential: a genuine tool to quantify functional connectivity. PLoS One 13:e0209001.

Montgomery SM, Sirota A, Buzsaki G (2008) Theta and gamma coordination of hippocampal networks during waking and rapid eye movement sleep. J Neurosci 28:6731–6741.

Nazari M, Karimi Abadchi J, Naghizadeh M, Bermudez-Contreras EJ, McNaughton BL, Tatsuno M, Mohajerani MH (2023) Regional variation in cholinergic terminal activity determines the non-uniform occurrence of cortical slow waves during REM sleep in mice. Cell Rep 42:112450.

Paxinos G, Franklin KBJ (2001) *The mouse brain in stereotaxic coordinates*, Ed. 2. San Diego, CA: Academic Press.

Peter-Derex L, Avigdor T, Rheims S, Guénot M, Von Ellenrieder N, Gotman J, Frauscher B (2023) Enhanced thalamocortical functional connectivity during rapid-eye-movement sleep sawtooth waves. Sleep 46:zsad097.

Petersen CCH, Hahn TTG, Mehta M, Grinvald A, Sakmann B (2003) Interaction of sensory responses with spontaneous depolarization in layer 2/3 barrel cortex. Proc Natl Acad Sci U S A 100:13638–13643.

Pinault D (1996) A novel single-cell staining procedure performed in vivo under electrophysiological control: morpho-functional features of juxtacellularly labeled thalamic cells and other central neurons with biocytin or neurobiotin. J Neurosci Methods 65:113–136.

Poe GR (2017) Sleep is for forgetting. J Neurosci 37:464–473.

Pophale A, et al. (2023) Wake-like skin patterning and neural activity during octopus sleep. Nature 619:129–134.

Rasch B, Born J (2013) About sleep's role in memory. Physiol Rev 93:681–766.

Rosier M, Le Barillier L, Meunier D, El Yacoubi M, Malleret G, Salin P-A (2018) Post-learning paradoxical sleep deprivation impairs reorganization of limbic and cortical networks associated with consolidation of remote contextual fear memory in mice. Sleep 41:1–18.

Sánchez-López A, Escudero M (2011) Tonic and phasic components of eye movements during REM sleep in the rat. Eur J Neurosci 33:2129–2138.

Sano K, Iwahara S, Senba K, Sano A, Yamazaki S (1973) Eye movements and hippocampal theta activity in rats. Electroencephalogr Clin Neurophysiol 35:621–625.

Sara SJ (2017) Sleep to remember. J Neurosci 37:457–463.

Sato S, Kanbayashi T, Kondo H, Matsubuchi N, Ono K, Shimizu T (2010) Rapid increase to double breathing rate appears during REM sleep in synchrony with REM –a higher CNS control of breathing? In: *New frontiers in respiratory control* (Homma I, Onimaru H, Fukuchi Y, eds), Advances in experimental medicine and biology. pp 249–252. New York, NY: Springer.

Sei H, Morita Y (1996) Effect of ambient temperature on arterial pressure variability during sleep in the rat. J Sleep Res 5:37–41.

Senzai Y, Scanziani M (2022) A cognitive process occurring during sleep is revealed by rapid eye movements. Science 377:999–1004.

Simor P, Gombos F, Szakadát S, Sándor P, Bódizs R (2016) EEG spectral power in phasic and tonic REM sleep: different patterns in young adults and children. J Sleep Res 25:269–277.
Simor P, Van Der Wijk G, Nobili L, Peigneux P (2020) The microstructure of REM sleep: why phasic and tonic? Sleep Med Rev 52:101305.
Sirota A, Csicsvari J, Buhl D, Buzsáki G (2003) Communication between neocortex and hippocampus during sleep in rodents. Proc Natl Acad Sci U S A 100:2065–2069.
Sirota A, Montgomery S, Fujisawa S, Isomura Y, Zugaro M, Buzsáki G (2008) Entrainment of neocortical neurons and gamma oscillations by the hippocampal theta rhythm. Neuron 60:683–697.
Soh K, Morita Y, Sei H (1992) Relationship between eye movements and oneiric behavior in cats. Physiol Behav 52:553–558.
Sprenger A, Lappe-Osthege M, Talamo S, Gais S, Kimmig H, Helmchen C (2010) Eye movements during REM sleep and imagination of visual scenes. Neuroreport 21:45–49.
Tinguely G, Finelli LA, Landolt H-P, Borbély AA, Achermann P (2006) Functional EEG topography in sleep and waking: state-dependent and state-independent features. Neuroimage 32:283–292.
Tiriac A, Blumberg MS (2016) The case of the disappearing spindle burst. Neural Plast 2016:8037321.
Tiriac A, Uitermarkt BD, Fanning AS, Sokoloff G, Blumberg MS (2012) Rapid whisker movements in sleeping newborn rats. Curr Biol 22:2075–2080.
Tononi G, Massimini M (2008) Why does consciousness fade in early sleep ? Ann N Y Acad Sci 1129:330–334.
Tort ABL, Fontanini A, Kramer MA, Jones-Lush LM, Kopell NJ, Katz DB (2010) Cortical networks produce three distinct 7–12 Hz rhythms during single sensory responses in the awake rat. J Neurosci 30:4315–4324.
Türker B, et al. (2023) Behavioral and brain responses to verbal stimuli reveal transient periods of cognitive integration of the external world during sleep. Nat Neurosci 26:1981–1993.
Urbain N, Fourcaud-Trocmé N, Laheux S, Salin PA, Gentet LJ (2019) Brain-state-dependent modulation of neuronal firing and membrane potential dynamics in the somatosensory thalamus during natural sleep. Cell Rep 26:1443–1457.
Urbain N, Salin PA, Libourel P-A, Comte J-C, Gentet LJ, Petersen CCH (2015) Whisking-related changes in neuronal firing and membrane potential dynamics in the somatosensory thalamus of awake mice. Cell Rep 13:647–656.
Vanni-Mercier G, Pelisson D, Goffart L, Sakai K, Jouvet M (1994) Eye saccade dynamics during paradoxical sleep in the cat. Eur J Neurosci 6:1298–1306.
Varela F, Lachaux J-P, Rodriguez E, Martinerie J (2001) The brainweb: phase synchronization and large-scale integration. Nat Rev Neurosci 2:229–239.
Veinante P, Jacquin MF, Deschênes M (2000) Thalamic projections from the whisker-sensitive regions of the spinal trigeminal complex in the rat. J Comp Neurol 420:233–243.
Vyazovskiy VV, Olcese U, Hanlon EC, Nir Y, Cirelli C, Tononi G (2011) Local sleep in awake rats. Nature 472:443–447.
Wehrle R, Kaufmann C, Wetter TC, Holsboer F, Auer DP, Pollmächer T, Czisch M (2007) Functional microstates within human REM sleep: first evidence from fMRI of a thalamocortical network specific for phasic REM periods: thalamocortical network in phasic REM sleep. Eur J Neurosci 25:863–871.
Wimmer RD, Astori S, Bond CT, Rovó Z, Chatton J-Y, Adelman JP, Franken P, Lüthi A (2012) Sustaining sleep spindles through enhanced SK2-channel activity consolidates sleep and elevates arousal threshold. J Neurosci 32:13917–13928.